Measurement-Conditioned Coherent Control: Driving-Speed and Measurement-Basis Optimization in Quantum Heat Engines

Yerong Li(李烨蓉), Yingying Hong(洪莹莹), Weiwei Zhang(张伟伟), and Jianhui Wang(王建辉)*

Department of Physics, Nanchang University, Nanchang 330031, China

(Received 24 December 2025; accepted manuscript online 18 March 2026)

We theoretically propose a cyclic quantum engine in which a single-qubit working medium undergoes finite-time unitary strokes with adjustable durations, followed by a projective measurement and an outcome-dependent coherent pulse (π or $\pi/2$ rotation). The protocol separates two independent control handles: the unitary driving speed $\tau_{\rm dr}$, which governs nonadiabatic transitions and phase accumulation, and the measurement parameter θ, which sets the outcome probabilities and the magnitude of measurement-induced energy injection. Feedback functions solely through pulses without altering the stroke time. Including the measurement and erasure costs, we show that the coordinated tuning of $\tau_{\rm dr}$ and θ yields substantial and robust gains in terms of power and efficiency.

DOI: 10.1088/0256-307X/43/4/040005 CSTR: 32039.14.0256-307X.43.4.040005

Introduction. Quantum heat engines extend classical thermodynamic principles into the quantum domain.[1–12] They provide a framework for investigating how genuinely quantum features, such as coherence,[13–28] entanglement,[9,29–36] and measurement information,[30,37–42] can serve as thermodynamic resources. In classical engines, performance is limited by a fundamental tradeoff between cycle time and dissipation:[43–45] rapid driving increases power but induces irreversible losses, whereas slow driving suppresses dissipation and reduces power output. However, in quantum systems, additional resources such as squeezing,[46] coherence,[23,47–51] and inner friction[52] can be harnessed to enhance the work extraction under certain conditions.

Measurement-based feedback is a promising strategy for controlling quantum coherence.[25,53–59] In such protocols, the working medium is first measured, and the measurement outcome guides the subsequent control operation. This process allows energy and coherence to be selectively injected, thus enabling the conversion of measurement-induced state changes into useful work. However, the benefits of this approach must be balanced with the energy cost of information processing, including the Landauer cost of memory erasure.[36,60–67]

Most previous studies on quantum coherence in engines focused on its passive role, in which coherence arises naturally during finite-time unitary strokes.[24,51,68–70] In this study, we propose an active scheme in which the unitary strokes retain a fixed duration while a measurement-conditioned coherent operation is applied prior to thermalization. Specifically, a projective measurement is performed on a tunable basis and parameterized by an angle θ, followed by an outcome-dependent pulse, i.e., a π pulse for one outcome and a $\pi/2$ pulse for another. These conditional operations modify the population and coherence of the working medium in a controlled manner, thereby enabling additional work extraction without altering the stroke duration.

Herein, we introduce a speed-controlled, measurement-conditioned feedback scheme for a cyclic quantum heat engine. The protocol is governed by two independent control parameters: the finite-time driving duration $\tau_{\rm dr}$ and the measurement-basis angle θ. Collectively, they determine the manner by which population and coherence are shaped before thermalization. The combination of finite-time driving and outcome-dependent pulses results in phase-sensitive coherences that interfere constructively or destructively, thereby resulting in oscillatory enhancements to the extractable work. When accounting for both measurement costs and Landauer erasure, we demonstrate that the joint optimization of $\tau_{\rm dr}$ and θ improves both power and efficiency significantly.

Feedback-Driven Engine. We present a feedback-driven quantum heat engine that operates with a single qubit as the working medium and follows a closed cyclic thermodynamic protocol. The engine comprises five distinct strokes: an isochoric thermalization process; an isochoric process, in which the system interacts weakly with a coherent laser field; two coherent unitary transformations (compression and expansion); and a measurement-feedback stage. Specifically, feedback is implemented via real-time control of both the interaction duration with the optical field and the time allocated for unitary expansion, based on the outcome of a projective quantum measurement. This dynamic adjustment enables precise control over both the energy exchange and quantum coherence generation throughout the engine cycle. The working principle of the engine is illustrated schematically in Fig. 1. The complete

*Corresponding author. Email: wangjianhui@ncu.edu.cn

© 2026 Chinese Physical Society and IOP Publishing Ltd. All rights, including for text and data mining, AI training, and similar technologies, are reserved.

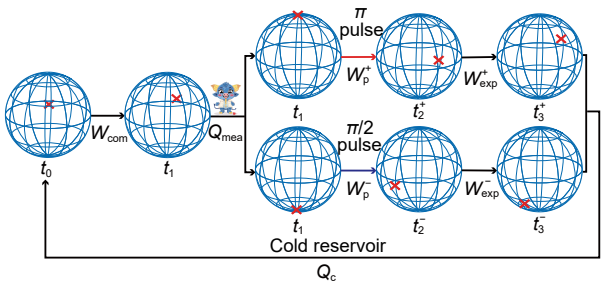

Fig. 1. Bloch-sphere representation of feedback-driven quantum engine cycle. Beginning from thermal equilibrium with a cold reservoir at t_0, the qubit undergoes unitary compression ($t_0 \to t_1$) and performs work $W_{\rm com}$ as the gap increases from $\omega_{\rm c}$ to $\omega_{\rm h}$. Subsequently, projective measurement in basis θ is performed at a fixed Hamiltonian, thus yielding outcomes $|\psi_\pm(\theta)\rangle$ at $t_1^\pm$. This measurement-and-feedback stage constitutes an isochoric coherent-control process, during which conditional π or $\pi/2$ pulses inject work $W_{\rm p}^\pm$. The subsequent unitary expansion ($t_2^\pm \to t_3^\pm$) extracts work $W_{\rm exp}$, and the final thermalization with the cold reservoir releases heat $Q_{\rm c}$, thereby completing the cycle.

thermodynamic cycle is described stepwise as follows.

Unitary compression process (t_0 to t_1; duration $\tau_{\rm com} = t_1 - t_0$). The cycle begins with adiabatic compression, during which the characteristic frequency of the system is ramped smoothly from $\omega_{\rm c}$ to $\omega_{\rm h}$ ($\omega_{\rm h} > \omega_{\rm c}$). This modulation effectively increases the energy-level spacing of the qubit. The time-dependent Hamiltonian used during this stage is expressed as ($\hbar \equiv 1$)

$$H_{\rm com}(t) = \frac{\omega_t}{2}\left[\cos\left(\frac{\pi t}{2\tau_{\rm com}}\right)\sigma_x + \sin\left(\frac{\pi t}{2\tau_{\rm com}}\right)\sigma_z\right], \quad (1)$$

with a linearly interpolated frequency $\omega_t = \omega_{\rm c}(1 - t/\tau_{\rm com}) + \omega_{\rm h}(t/\tau_{\rm com})$ for $t \in [0, \tau_{\rm com}]$. Here, σ_x and σ_z are Pauli matrices, with $\sigma_z = |e\rangle\langle e| - |g\rangle\langle g|$. The rotating structure expressed in Eq. (1) corresponds to an effective field whose orientation changes smoothly over time, thus inducing nonadiabatic transitions and coherence between instantaneous energy eigenstates for a finite driving duration. In the adiabatic limit, such coherences vanish, whereas in finite-time driving, they become a key resource for work extractions and enable controlled finite-time driving. The Hamiltonian form is widely used in both theoretical and experimental studies of finite-time quantum thermodynamics and quantum friction, and can be readily implemented in platforms such as nuclear magnetic resonance and superconducting qubits (see Refs. [52,71]).

The system initially begins in thermal equilibrium with the cold reservoir, which is described by the Gibbs state $\rho_{t_0}^{\rm eq} = {\rm e}^{-\beta_{\rm c}H(t_0)}/{\rm Tr}[{\rm e}^{-\beta_{\rm c}H(t_0)}]$, with an inverse temperature ($k_{\rm B} \equiv 1$) $\beta_{\rm c} = 1/T_{\rm c}$. Subsequently, the state evolves unitarily to $\rho_{t_1} = U_{\rm com}\rho_{t_0}^{\rm eq}U_{\rm com}^\dagger$ with $U_{\rm com} = \vec{\mathcal{T}}\exp[-{\rm i}\int_{t_0}^{t_1}{\rm d}t\, H_{\rm com}(t)]$, where $\vec{\mathcal{T}}$ is the time-ordered evolution operator.

Projective measurements (negligible duration). At $t = t_1$, a projective measurement was performed on a tunable basis, thus projecting the system into one of two pure states. The basis states are expressed as follows:[25,72,73]

$$\begin{aligned}|\psi_+(\theta)\rangle &= \cos\frac{\theta}{2}|e\rangle + \sin\frac{\theta}{2}|g\rangle,\\ |\psi_-(\theta)\rangle &= \sin\frac{\theta}{2}|e\rangle - \cos\frac{\theta}{2}|g\rangle,\end{aligned} \quad (2)$$

where $\theta \in [0, \pi/2]$ controls the measurement axis. The measurement collapses the state to $\rho_{t_1}^m = |\psi_m\rangle\langle\psi_m|$ with probability

$$q_m = \langle\psi_m|\rho_{t_1}|\psi_m\rangle, \quad (3)$$

where $m = \pm$. A larger value of θ increases the probability of the outcome $|\psi_+\rangle$, thus shifting the population bias toward the excited state $|e\rangle$. This tuning of θ allows control over the measurement probabilities q_+ and q_-, which are determined by the overlap of the state with the measurement basis, as shown in Eq. (3). Measurements in bases misaligned with the Hamiltonian direction introduce energetic disturbances and changes in entropy. The entropy change is expressed as

$$\Delta S = \sum_m q_m S[\rho_{t_1}^m] - S[\rho_{t_1}] = {\rm Tr}(\rho_{t_1}\ln\rho_{t_1}), \quad (4)$$

since pure post-measurement states have zero entropy. This entropy change is essential for understanding the thermodynamic cost of information acquisition.

Interaction with laser pulse (t_1 to t_2^m; duration $\tau_{\rm p}^m = t_2^m - t_1$). Following the measurement, the system interacts with a coherent laser field of outcome-dependent duration $\tau_{\rm p}^m = t_2^m - t_1$ under a fixed Hamiltonian $H = H_{\rm h} = \omega_{\rm h}\sigma_z/2$. The time evolution is governed by the Liouville-von Neumann equation as follows:[25,74]

$$\partial_t\rho_t^m = -{\rm i}[\widetilde{H}_{\rm p}(t), \rho_t^m], \quad (5)$$

with

$$\widetilde{H}_{\rm p}(t) = H_{\rm h} + \frac{\Omega}{2}\left({\rm e}^{-{\rm i}(\omega_{\rm h}t-\phi)}|e\rangle\langle g| + {\rm H.c.}\right), \quad (6)$$

where Ω is the Rabi frequency and ϕ is the phase of the driving field. The system undergoes a coherent evolution expressed as

$$\rho_{t_2}^m = U_{\rm p}^m\rho_{t_1}^m(U_{\rm p}^m)^\dagger, \quad (7)$$

with

$$\begin{aligned}&U_{\rm p}^m\\ &= \cos\left(\frac{\Omega\tau_{\rm p}^m}{2}\right)\left({\rm e}^{{\rm i}\omega_{\rm h}\tau_{\rm p}^m/2}|g\rangle\langle g| + {\rm e}^{-{\rm i}\omega_{\rm h}\tau_{\rm p}^m/2}|e\rangle\langle e|\right)\\ &\quad - {\rm i}\sin\left(\frac{\Omega\tau_{\rm p}^m}{2}\right)\left({\rm e}^{{\rm i}(\omega_{\rm h}\tau_{\rm p}^m/2-\phi)}L^\dagger + {\rm e}^{-{\rm i}(\omega_{\rm h}\tau_{\rm p}^m/2-\phi)}L\right),\end{aligned} \quad (8)$$

where $L = |e\rangle\langle g|$ and $L^\dagger = |g\rangle\langle e|$. This interaction extracts work, depending on the measurement outcome.

Unitary expansion process (t_2^m to t_3^m; duration $\tau_{\rm exp}^m = t_3^m - t_2^m$). Here, the expansion duration $\tau_{\rm exp}^m$ generally depends on the measurement outcome m. In particular, we denote $\tau_{\rm exp}^+$ and $\tau_{\rm exp}^-$ as the expansion times conditioned on outcomes $+$ and $-$, respectively. Following the compression stroke, the system undergoes a finite-time unitary expansion designed as the time-reversed counterpart of the compression protocol. Specifically, the expansion Hamiltonian satisfies $H_{\rm exp}(t') = -H_{\rm com}(\tau_{\rm com} - t')$, for

$0 \le t' \le \tau_{\rm com}$, which ensures that the corresponding propagators obey $U_{\rm exp} = U_{\rm com}^{\dagger}$. Compression and expansion strokes are performed for the same duration. Therefore, we introduce a common driving time $\tau_{\rm dr} \equiv \tau_{\rm com} = \tau_{\rm exp}^{\pm}$.

The Hamiltonian governing the expansion stage is expressed as

$$H_{\rm exp}(t') = -\frac{\omega_{t'}}{2}\left[\sin\left(\frac{\pi t'}{2\tau_{\rm dr}}\right)\sigma_x + \cos\left(\frac{\pi t'}{2\tau_{\rm dr}}\right)\sigma_z\right], \quad (9)$$

where $t' = t - t_2^m$ with $t_2^m \le t \le t_3^m$ denotes the time elapsed since the beginning of the expansion stroke. The instantaneous frequency varies linearly from $\omega_{\rm h}$ to $\omega_{\rm c}$ according to

$$\omega_{t'} = \omega_{\rm h}\left(1 - \frac{t'}{\tau_{\rm dr}}\right) + \omega_{\rm c}\left(\frac{t'}{\tau_{\rm dr}}\right). \quad (10)$$

Therefore, the state at the end of the expansion stroke is

$$\rho_{t_3}^m = U_{\rm exp}^m \rho_{t_2}^m \left(U_{\rm exp}^m\right)^{\dagger}, \quad (11)$$

where $U_{\rm exp}^m = \vec{\mathcal{T}} \exp\left[-{\rm i}\int_{t_2^m}^{t_3^m} H_{\rm exp}(t)\,{\rm d}t\right]$ is the time-ordered unitary propagator. In practice, the density operators in Eqs. (7) and (11) are obtained by numerically constructing the corresponding time-ordered propagators generated by the prescribed time-dependent Hamiltonians and applying the unitary transformation $\rho \to U\rho U^{\dagger}$.

Throughout the cycle, the system dynamics are governed by finite-time unitary evolution: the short laser pulse induces a simple rotation of the quantum state, whereas the compression and expansion strokes are driven by nonperiodic control and are thus described by direct time evolution instead of a Floquet approach.

Isochoric cooling stage. Finally, the system is coupled to a cold reservoir, where it undergoes complete thermalization. The dynamics are governed by the Lindblad master equation as follows:[75,76]

$$\begin{aligned}\frac{{\rm d}\rho_t^m}{{\rm d}t} &= -{\rm i}[H_{\rm exp}(t), \rho_t^m] + \gamma_{\rm c} N_{\rm c}\left(L\rho_t^m L^{\dagger} - \tfrac{1}{2}\{L^{\dagger}L, \rho_t^m\}\right) \\ &\quad + \gamma_{\rm c}(N_{\rm c}+1)\left(L^{\dagger}\rho_t^m L - \tfrac{1}{2}\{LL^{\dagger}, \rho_t^m\}\right), \end{aligned} \quad (12)$$

where $N_{\rm c} = [\exp(\beta_{\rm c}\omega_{\rm c}) - 1]^{-1}$ denotes the thermal photon number and $\gamma_{\rm c}$ is the coupling strength. The relaxation process can be represented by a fixed duration $\tau_{\rm c}$, which is independent of the initial state, provided $\tau_{\rm c}$ is selected to be sufficiently long [see the Supplemental Material (SM) for details,[77] which includes Ref. [14]]. This step restores the engine to its initial thermal state and completes the cycle. We consider an engine operating in the limit cycle regime,[78] where a periodic steady state is reached and all the state variables become time periodic.

The total cycle duration is determined by the feedback outcomes and is expressed as

$$\tau_{\rm cyc} = \sum_{m=\pm} q_m \tau_{\rm p}^m + 2\tau_{\rm dr} + \tau_{\rm c}, \quad (13)$$

this expression highlights the manner by which the measurement-induced feedback controls the timing of the thermodynamic cycle. The cycle duration $\tau_{\rm cyc}$ in Eq. (13) is an ensemble-averaged quantity: the projective measurement yields outcomes $m = \pm$ with probabilities q_m, each followed by a feedback pulse of duration $\tau_{\rm p}^m$.

In each cycle, the internal energy at time t is expressed as $E_t = {\rm Tr}[\rho_t H(t)] = \langle n(t)\rangle\,\omega_t$, where $\langle n(t)\rangle = \frac{1}{2}{\rm Tr}[\rho_t\,(|e(t)\rangle\langle e(t)| - |g(t)\rangle\langle g(t)|)]$ (or $\langle n_m(t)\rangle = \frac{1}{2}{\rm Tr}[\rho_t^m\,(|e(t)\rangle\langle e(t)| - |g(t)\rangle\langle g(t)|)]$) denotes the instantaneous population imbalance between the excited and ground states. Using this formal description of the system state ρ_t, the work and heat exchanged in each stroke can be computed. The work input during compression, $W_{\rm com}$, the measurement energy cost treated as heat,[79] $Q_{\rm mea}$, the work input during the system-field interaction, $W_{\rm p}^m$, and the work input during the unitary expansion, $W_{\rm exp}^m$, are expressed as follows (see the SM for detailed derivations[77]):

$$W_{\rm com} = \langle n(t_0)\rangle\,[\omega_{\rm h}(1 - 2\xi_{\rm com}) - \omega_{\rm c}], \quad (14)$$

$$\begin{aligned} Q_{\rm mea} &= \big[q_+\langle n_+(t_1)\rangle + q_-\langle n_-(t_1)\rangle \\ &\quad + \langle n(t_0)\rangle(-1 + 2\xi_{\rm com})\big]\omega_{\rm h}, \end{aligned} \quad (15)$$

$$\begin{aligned} W_{\rm p}^m &= \omega_{\rm h}\Big\{\langle n_m(t_1)\rangle\,\big[\cos(\Omega\tau_{\rm p}^m) - 1\big] \\ &\quad - \sin(\Omega\tau_{\rm p}^m)\,{\rm Re}\big[{\rm i}\rho_{ge}^m(t_1){\rm e}^{{\rm i}\phi}\big]\Big\}, \end{aligned} \quad (16)$$

$$\begin{aligned} W_{\rm exp}^m &= \Big[\omega_{\rm h} - \omega_{\rm c}\big(1 - 2\xi_{\rm exp}^m\big)\Big]\Big\{\sin\big(\Omega\tau_{\rm p}^m\big)\,{\rm Re}\Big[{\rm i}\rho_{ge}^m(t_1){\rm e}^{{\rm i}\phi}\Big] \\ &\quad - \langle n_m(t_1)\rangle\cos\big(\Omega\tau_{\rm p}^m\big)\Big\} - 2\omega_{\rm c}\chi_{\rm exp}^m, \end{aligned} \quad (17)$$

where the adiabaticity parameters $\xi_{\rm com} = |\langle e|U_{\rm com}|g\rangle|^2$, $\xi_{\rm exp}^m = |\langle e|U_{\rm exp}^m|g\rangle|^2$ measure the transition probability between energy eigenstates. The coherence parameter $\chi_{\rm exp}^m = {\rm Re}\Big[U_{\rm exp}^{gg}\langle g|\rho_{t_2}^m|e\rangle\left(U_{\rm exp}^{eg}\right)^{\dagger}\Big]$ accounts for the contribution of quantum coherence to the expansion work.

The compression and expansion Hamiltonians are exact time-reverses with identical durations. Consequently, their unitary propagators yield transition amplitudes that are complex conjugates. Physically, this implies that the expansion stroke exactly reverses the compression dynamics, thus guaranteeing equal transition probabilities. Therefore, we define a unified adiabaticity parameter $\xi \equiv \xi_{\rm com} = \xi_{\rm exp}^m$ for both strokes.[52,71] The coherence generated during the system-field interaction is captured by ${\rm Re}\big[{\rm i}\rho_{ge}^m(t_1){\rm e}^{{\rm i}\phi}\big]$, while $\chi_{\rm exp}^m$ quantifies the coherence yielded during the subsequent unitary expansion for outcome m. Both coherences originate from the unitary strokes and phase accumulation, and both directly determine the work output.

Using Eqs. (14), (16), and (17), the total work output per cycle is expressed as

$$-W = -W_{\rm com} - \sum_m q_m\left(W_{\rm p}^m + W_{\rm exp}^m\right), \quad (18)$$

where q_m is expressed as shown in Eq. (3). The corresponding power output is $P = -W/\tau_{\rm cyc}$.

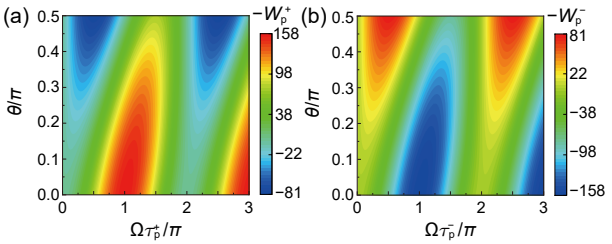

Fig. 2. (a) Contour plot of work output $-W_{\rm p}^{+}$ and (b) $-W_{\rm p}^{-}$ generated during interaction between the system and optical field. Work is plotted as a function of the pulse area $\Omega\tau_{\rm p}^{m}$ and control parameter θ, with the drive duration fixed at $\tau_{\rm dr} = 0.036$. The parameters are as follows: $\omega_{\rm h} = 50\pi$, $\omega_{\rm c} = 0.4\,\omega_{\rm h}$, $\beta_{\rm c} = 2/\omega_{\rm c}$, $\Omega = \phi = 0.5\pi$, $\gamma_{\rm c} = 1$, and $\tau_{\rm c} = 5$.

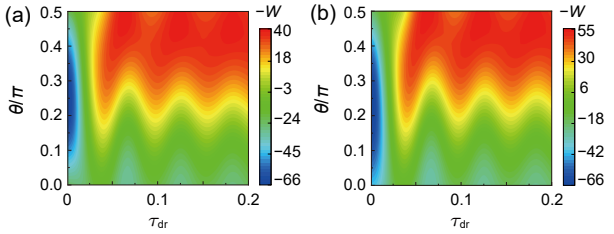

Fig. 3. (a) Contour plot of total average work $-W$ performed by system without feedback, shown as a function of adiabatic driving time $\tau_{\rm dr}$ and control parameter θ, with $\Omega\tau_{\rm p}^{+} = \Omega\tau_{\rm p}^{-} = 0.5\pi$. (b) Same plot under feedback control, with $\Omega\tau_{\rm p}^{+} = \pi$ and $\Omega\tau_{\rm p}^{-} = 0.5\pi$. All other parameters are identical to those used in Fig. 2.

The work input during the interaction between the system and optical field, denoted as $W_{\rm p}^{m}$ and expressed in Eq. (16), occurs over the controlled interaction duration $\tau_{\rm p}^{m}$. This input depends sensitively on the initial quantum state of the system $\rho_{t_1}^{m}$, which is determined by the outcome $m = \pm$ of the preceding measurement. Crucially, the amount of work injected can be regulated dynamically by adjusting the duration $\tau_{\rm p}^{m}$ of the optical pulse. This controllability introduces a practical approach for optimizing energy transfer.

As shown in Fig. 2, the injected work $W_{\rm p}^{\pm}$ exhibits pronounced periodic oscillations as a function of the dimensionless pulse area $\Omega\tau_{\rm p}^{m}$, where Ω denotes the coupling strength. Notably, the values of $\Omega\tau_{\rm p}^{+}$ and $\Omega\tau_{\rm p}^{-}$ that maximize $W_{\rm p}^{+}$ [Fig. 2(a)] and $W_{\rm p}^{-}$ [Fig. 2(b)] are almost independent of the measurement parameter θ [see Eq. (2)]. This weak sensitivity to θ demonstrates the robustness of the control protocol and indicates that the energy injected by the pulse can be efficiently regulated via the pulse duration alone. Subsequently, based on Fig. 2, although the measurement-conditioned pulses satisfy $W_{\rm p}^{+} + W_{\rm p}^{-} = 0$ because of the antisymmetric structure of the post-measurement states (a detailed derivation is provided in the SM), their probability-weighted average is generally nonzero, i.e., $q_{+}W_{\rm p}^{+} + q_{-}W_{\rm p}^{-} \neq 0$. Our feedback protocol capitalizes on this imbalance by applying outcome-dependent pulses, thereby converting the measurement backaction into useful work while fully preserving the overall energy conservation.

This observation motivated the development of a simple yet effective feedback protocol. When the system is projected into state $\rho_{t_1}^{+}$, the pulse duration $\tau_{\rm p}^{+}$ is selected to correspond to a π-pulse, thus achieving complete population inversion and maximizing photon absorption. Conversely, when the system is projected into $\rho_{t_1}^{-}$, a $\pi/2$-pulse of duration $\tau_{\rm p}^{-}$ is applied to ensure optimal energy injection without overdriving the transition. By conditionally applying either a π- or $\pi/2$-pulse based on the measurement outcome, the system efficiently absorbs energy from the external optical cavity.

The interaction interval between the system and control pulse, as determined by the feedback mechanism, is crucial for defining the initial conditions for the subsequent unitary expansion stroke. In our model, feedback control is implemented as follows: if the measurement outcome yields the state $\rho_{t_1}^{+} = |\psi_{+}\rangle\langle\psi_{+}|$, then a π-pulse is applied to the qubit system; and if the outcome is $\rho_{t_1}^{-} = |\psi_{-}\rangle\langle\psi_{-}|$, then a $\pi/2$ pulse is applied. This selective use of control pulses directly determines the initial state for expansion and thus modifies the work output in this stage. For the π-pulse interaction, equation (17) is reduced to $W_{\rm exp}^{+} = [\omega_{\rm h} - \omega_{\rm c}\,(1-\xi)]\,\langle n_{+}(t_1)\rangle - 2\omega_{\rm c}\chi_{\rm exp}^{+}$, where the work output depends explicitly on the system frequency and the feedback-modulated parameter ξ. By contrast, for a $\pi/2$-pulse interaction, equation (17) is simplified to $W_{\rm exp}^{-} = [\omega_{\rm h} - \omega_{\rm c}\,(1-2\xi)]\,{\rm Re}\big[{\rm i}\rho_{ge}^{-}(t_1){\rm e}^{{\rm i}\phi}\big] - 2\omega_{\rm c}\chi_{\rm exp}^{-}$, thus reflecting a partial state rotation. In our engine, selectively applying these pulses based on the measurement outcome allows the average work output $-W$, as expressed in Eq. (18), to be decomposed into distinct physical contributions as follows: $-W = W_{\rm qua} + W_{\rm fri} + W_{\rm coh}$.

Here, the coherent work is expressed as

$$W_{\rm coh} = 2q_{+}\omega_{\rm c}\chi_{\rm exp}^{+} + 2q_{-}\omega_{\rm c}\chi_{\rm exp}^{-}, \tag{19}$$

and is associated with the quantum coherence generated during the expansion and compression strokes. The term

$$\begin{aligned} W_{\rm fri} \;=\; & 2\langle n(t_0)\rangle\omega_{\rm h}\xi - 2\omega_{\rm c}\xi q_{+}\langle n_{+}(t_1)\rangle \\ & - 2\omega_{\rm c}\xi q_{-}{\rm Re}[{\rm i}\rho_{ge}^{-}(t_1){\rm e}^{{\rm i}\phi}], \end{aligned} \tag{20}$$

represents the contribution from quantum friction arising from the non-adiabatic expansion and compression processes, whereas

$$\begin{aligned} W_{\rm qua} \;=\; & (\omega_{\rm c} - \omega_{\rm h})\{\langle n(t_0)\rangle + q_{+}\langle n_{+}(t_1)\rangle \\ & + q_{-}{\rm Re}[{\rm i}\rho_{ge}^{-}(t_1){\rm e}^{{\rm i}\phi}]\} + 2q_{+}\omega_{\rm h}\langle n_{+}(t_1)\rangle \\ & + 2q_{-}\omega_{\rm h}\{\frac{\sqrt{2}}{2}\langle n_{-}(t_1)\rangle + {\rm Re}[{\rm i}\rho_{ge}^{-}(t_1){\rm e}^{{\rm i}\phi}]\}, \end{aligned} \tag{21}$$

corresponds to quasistatic work in the limit where both unitary strokes satisfy the long-time, quasistatic condition.

Figure 3 presents the total average work output $-W$ as a function of the adiabatic driving time $\tau_{\rm dr}$ and the control parameter θ for two cases: without feedback [Fig. 3(a)] and with feedback [Fig. 3(b)]. A direct comparison shows that introducing feedback substantially enhances the work output over a broad range of $(\tau_{\rm dr}, \theta)$. In contrast to the no-feedback case, where the performance is limited by unitary driving alone, measurement-conditioned feedback enables additional work extraction by converting

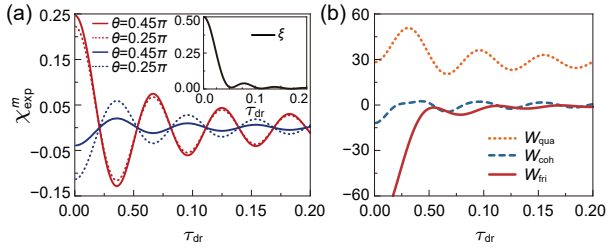

Fig. 4. (a) Parameter $\chi^m_{\rm exp}$ vs. driving time $\tau_{\rm dr}$ during unitary expansion. Inset: Adiabaticity parameter ξ vs. $\tau_{\rm dr}$. Solid ($\theta = 0.45\pi$) and dashed ($\theta = 0.25\pi$) red lines show $\chi^+_{\rm exp}$; blue counterparts show $\chi^-_{\rm exp}$. (b) Work components vs. $\tau_{\rm dr}$ for $\theta = 0.25\pi$: quasistatic ($W_{\rm qua}$), coherent ($W_{\rm coh}$), and frictional ($W_{\rm fri}$). For both panels, $\Omega\tau_{\rm p}^+ = \pi$, $\Omega\tau_{\rm p}^- = 0.5\pi$, with other parameters matching Fig. 2.

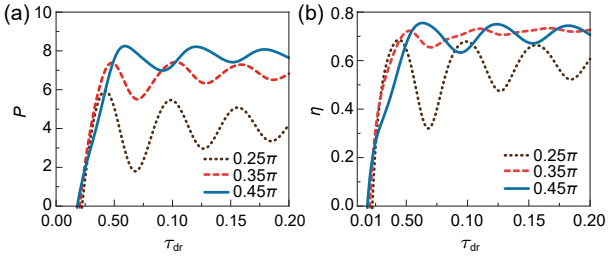

Fig. 5. (a) Power output P and (b) efficiency η as functions of driving time $\tau_{\rm dr}$ for $\theta = 0.25\pi$, 0.35π, and 0.45π. The pulse parameters are $\Omega\tau_p^+ = \pi$ and $\Omega\tau_p^- = 0.5\pi$. All other parameters are the same as in Fig. 2.

measurement-induced energy into useful output through outcome-dependent control. Because the energetic costs of the measurement and information erasure are fully included in the thermodynamic analysis, the enhanced work output in the feedback-driven case constitutes a genuine thermodynamic advantage of the measurement-powered scheme.

The coherence parameter $\chi^m_{\rm exp}$ in Fig. 4(a), which is generated during unitary expansion and compression, exhibits periodic oscillations with the driving time $\tau_{\rm dr}$. These oscillations decrease in amplitude as $\tau_{\rm dr}$ increases, thus reflecting suppressed nonadiabatic transitions and convergence toward the adiabatic limit, where the population exchange between the energy eigenstates becomes negligible. Additionally, $\chi^m_{\rm exp}$ depends on the angle θ [Eq. (17)], which governs the coherence generated during the unitary expansion stroke, thereby affecting the interference pattern and the engine's output and efficiency. Byn contrast, the adiabaticity parameter ξ, which represents the transition probability between the ground and excited states, generally decreases with $\tau_{\rm dr}$ but shows nonmonotonic variations due to quantum interference, as shown in the inset of Fig. 4(a).

In Fig. 4(b), the frictional work $W_{\rm fri}$ becomes significant only under *ultrafast* driving, thus reflecting strong nonadiabatic effects from rapid driving. Outside this regime, both $W_{\rm fri}$ and the coherent contribution $W_{\rm coh}$ remain negligible. Consequently, the quasistatic work $W_{\rm qua}$ dominates for moderate-to-slow driving protocols. However, $W_{\rm qua}$ continues to vary with the driving time $\tau_{\rm dr}$ because of the state prepared by the measurement after finite-time compression. Coherences generated during the unitary compression—dependent on $\tau_{\rm dr}$—induce oscillations in $W_{\rm qua}$ via terms in Eq. (21) that depend on the coherence-sensitive probability parameter q_m. Thus, adjusting $\tau_{\rm dr}$ provides a practical method for enhancing engine's output without altering other parameters.

A complete thermodynamic cycle requires erasing the measurement record to prevent error accumulation. Without this erasure, the feedback protocols lose fidelity and the engine performance deteriorates. According to Landauer's principle, resetting one bit of memory incurs a thermodynamic cost: the environment must absorb at least ΔS of the entropy.[25,30] The corresponding energy dissipation is expressed as

$$Q_{\rm era} = -\Delta S/\beta_{\rm c}, \tag{22}$$

where ΔS is expressed as shown in Eq. (4), and this energy dissipation is transferred to the cold reservoir. This memory reset is essential for a reliable feedback control. Proper memory management ensures the long-term stability and reproducibility of the quantum engine's operation.

In addition to the power output, *efficiency*—defined as the ratio of work output to energy input—serves as a critical performance metric. This system exhibits fundamentally distinct efficiency characteristics compared with conventional heat engines that operate between hot and cold reservoirs. Although conventional efficiency calculations consider only heat absorbed from a high-temperature reservoir as the energy cost, our model incorporates two dissipation mechanisms: energy contributions from quantum measurements and information erasure. The efficiency is expressed as[80]

$$\eta = \frac{-W}{Q_{\rm mea} + Q_{\rm era}}, \tag{23}$$

where $-W$ denotes the total work output [Eq. (18)], $Q_{\rm mea}$ the measurement-induced energy [Eq. (15)], and $Q_{\rm era}$ the energy cost of information erasure [Eq. (22)].

Figure 5 presents the engine's performance based on two metrics, i.e., (a) the cycle-averaged power output P and (b) the thermodynamic efficiency η, each plotted as a function of the adiabatic driving time $\tau_{\rm dr}$ for three measurement angles $\theta = 0.25\pi$, 0.35π, and 0.45π. Both P and η exhibit pronounced nonmonotonic dependence on $\tau_{\rm dr}$. For an extremely short $\tau_{\rm dr}$, both become negative, thus indicating engine failure owing to significant frictional losses [see Fig. 4(b)]. As $\tau_{\rm dr}$ increases, friction-induced oscillations are suppressed, thus yielding a distinct P peak at an intermediate $\tau_{\rm dr}$. Beyond this peak, the power decreases because longer strokes extend the cycle time, thereby reducing the average output despite the lower dissipation.

The efficiency η shows a related but distinct trend. At a moderate $\tau_{\rm dr}$, the reduced friction and feedback-enhanced energy injection combine to increase the efficiency well above that of uncontrolled driving. However, η does not necessarily peak with P; instead, it reaches its maximum when the feedback work offsets the energetic costs of measurement and memory erasure. Thus, optimal

performance requires balancing friction suppression with the thermodynamic cost of information processing.

Similarly, the power and efficiency are determined by the measurement angle θ, which controls the feedback energy injection and coherence generation during the measurement stroke. Variations in the peak amplitudes across θ indicate that it is an effective tuning parameter that enables performance optimization while maintaining robustness to moderate changes. Thus, coherent control combined with measurement-based feedback can enhance both P and η. This underscores the necessity to optimize $\tau_{\rm dr}$ to limit nonadiabatic effects and select θ to balance feedback benefits with information-processing costs.

In addition to identifying the optimal operating points, figure 5 reveal that the engine performance is not confined to narrowly fine-tuned parameters. In fact, the protocol remains robust against realistic control imperfections, a property that is afforded by its structural design. First, the engine is governed by two independent control parameters, i.e., the driving duration $\tau_{\rm dr}$ and the measurement-basis angle θ, which collectively define a two-dimensional optimization landscape. As shown in Figs. 5(a) and 5(b), both the high power and appreciable efficiency persist over a finite range of $\tau_{\rm dr}$ for a fixed θ, thus indicating a broad operational bandwidth instead of a fragile optimum. As illustrated in Figs. 5(a) and 5(b), both high power and substantial efficiency are maintained over a finite interval of $\tau_{\rm dr}$ for a fixed θ, thus indicating a broad operational range instead of a sharply tuned optimum. The power and efficiency become negative only within a small region corresponding to extremely fast driving. In this regime, the frictional work dominates and contributes negatively, as shown in Fig. 4(b). Second, the projective measurement performed after each cycle resets the quantum phase, thereby suppressing the accumulation of phase errors. Consequently, dephasing during finite-time strokes minimally affects the engine performance, and slow parameter drifts can be mitigated by adjusting the measurement angle θ.

Discussions and Conclusions. The control ingredients assumed in our model are compatible with existing single-qubit platforms, where finite-time unitary driving and conditional π or $\pi/2$ pulses can be implemented using standard radiofrequency or microwave control.[25,48,52] Projective measurements on a tunable basis characterized by an angle θ can be realized through a suitable pre-rotation followed by conventional population readout schemes, as commonly employed in quantum measurement and control protocols.[37] The main experimental challenge is not the implementation of these controls but the consistent thermodynamic accounting of measurement and feedback, in particular, the measurement-induced energy $Q_{\rm mea}$ and the Landauer erasure cost $Q_{\rm era}$ entering the efficiency definition [Eq. (23)], which can be obtained using calorimetric approaches.[30,41] By restricting feedback to conditional coherent pulses while fixing the unitary stroke duration, the protocol reduces the real-time control complexity and enables a direct experimental test of the cooperative optimization of the driving speed $\tau_{\rm dr}$ and measurement-basis angle θ.

We introduced a speed-controlled, measurement-feedback quantum engine in which a single-qubit working medium undergoes finite-time driving, followed by projective measurements on a tunable basis and outcome-conditioned coherent pulses. Depending on the measurement result, either a π or $\pi/2$ pulse is applied, thus enabling targeted energy transfer or coherence conversion without altering the stroke duration. Finite-time driving generates $\tau_{\rm dr}$-dependent coherences whose interference with conditional pulses results in nonmonotonic variations in the cycle performance. The protocol uses two independent controls, i.e., the driving time $\tau_{\rm dr}$ and measurement -basis angle θ, to shape both the populations and phase-sensitive coherences before thermalization. More importantly, the projective measurement introduces an additional, information-controlled energy channel that is absent in purely unitary-driven cycles. Even after explicitly accounting for the thermodynamic costs of the measurement and Landauer erasure, this measurement-powered mechanism yields a net enhancement in work, power, and efficiency, thereby establishing a genuine thermodynamic advantage. Physically, the scheme exploits quantum coherence as an active thermodynamic resource—converting measurement-induced coherence into useful work—while mitigating nonadiabatic losses. This framework highlights the manner by which the coordinated control of unitary driving and feedback can enhance engine operation. Extending this approach to multilevel systems or many-body working media offers a promising route for scalable, high-performance quantum thermal machines.

Acknowledgements. This study was supported by the National Natural Science Foundation of China (Grant No. 12465009) and the Major Program of the Jiangxi Provincial Natural Science Foundation (Grant No. 20224ACB201007).

References

[1] Newman D, Mintert F, and Nazir A 2017 *Phys. Rev. E* **95** 032139
[2] Liu J and Jung K A 2024 *Phys. Rev. E* **109** 044118
[3] Boubakour M, Fogarty T, and Busch T 2023 *Phys. Rev. Res.* **5** 013088
[4] Ji W T, Chai Z H, Wang M Q, Guo Y H, Rong X, Shi F Z, Ren C L, Wang Y, and Du J F 2022 *Phys. Rev. Lett.* **128** 090602
[5] Campisi M, Pekola J, and Fazio R 2015 *New J. Phys.* **17** 035012
[6] Yuan J H, Ruan H L, Liu D H, He J Z, and Wang J H 2023 *Chin. Phys. Lett.* **40** 100502
[7] Miller H J D, Mohammady M H, Perarnau-Llobet M, and Guarnieri G 2021 *Phys. Rev. Lett.* **126** 210603
[8] Quan H T, Liu Y X, Sun C P, and Nori F 2007 *Phys. Rev. E* **76** 031105
[9] Kamimura S, Hakoshima H, Matsuzaki U, Yoshida K, and Tokura Y 2022 *Phys. Rev. Lett.* **128** 180602
[10] Liu D H, Hong Y Y, and Wang J H 2025 *Chin. Phys. Lett.* **42** 080001
[11] Zhang X Y, Liu Y, Cao X F, and He D H 2025 *Phys. Rev. B* **111** 235401

[12] Izumida Y, Okuda K, Roco J M M, and Calvo Hernández A 2015 *Phys. Rev. E* **91** 052140
[13] Baumgratz T, Cramer M, and Plenio M B 2014 *Phys. Rev. Lett.* **113** 140401
[14] Camati P A, Santos J F G, and Serra R M 2019 *Phys. Rev. A* **99** 062103
[15] Lu J, Wang Z, Ren J, Wang C, and Jiang J H 2024 *Phys. Rev. B* **109** 125407
[16] Aimet S and Kwon H 2023 *Phys. Rev. A* **107** 012221
[17] Scully M O, Chapin K R, Dorfman K E, Kim M B, and Svidzinsky A 2011 *Proc. Natl. Acad. Sci. U.S.A.* **108** 15097
[18] Um J, Dorfman K E, and Park H 2022 *Phys. Rev. Res.* **4** L032034
[19] Rahav S, Harbola U, and Mukamel S 2012 *Phys. Rev. A* **86** 043843
[20] Brandner K, Bauer M, and Seifert U 2017 *Phys. Rev. Lett.* **119** 170602
[21] Dorfman K E, Xu D, and Cao J 2018 *Phys. Rev. E* **97** 042120
[22] Tajima H and Takagi R 2025 *Phys. Rev. Lett.* **134** 170201
[23] Shi Y H, Shi H L, Wang X H, Hu M L, Liu S Y, Yang W L, and Fan H 2020 *J. Phys. A* **53** 085301
[24] Uzdin R 2016 *Phys. Rev. A* **6** 024004
[25] Brandner K, Bauer M, Schmid M T, and Seifert U 2015 *New J. Phys.* **17** 065006
[26] Prech K, Potts P P, and Landi G T 2025 *Phys. Rev. Lett.* **134** 020401
[27] Hu B Z, Nian L L, and Lü J T 2020 *Chin. Phys. B* **29** 120505
[28] Dai Y Q, Fu Y, Shi Z Y, Qin X, Mu S W, Wu Y, Su J H, Deng Y F, Qin L, and Zhai Y Q 2021 *Chin. Phys. Lett.* **38** 030303
[29] Wang K K, Xia R Q, Bresque L, and Xue P 2022 *Phys. Rev. Res.* **4** L032042
[30] Bresque L, Camati P A, Rogers S, Murch K, Jordan A N, and Auffèves A 2021 *Phys. Rev. Lett.* **126** 120605
[31] Wang Z, Deng Z H, Liu Z N, Wang Z Y, Ding Y M, Zhang L, Guo W N, and Yan Z 2025 *Chin. Phys. Lett.* **42** 110712
[32] Tavakoli A, Haack G, Brunner N, and Jonatan B B 2020 *Phys. Rev. A* **101** 012315
[33] Khandelwal S, Palazzo N, Brunner N, and Haack G 2020 *New J. Phys.* **22** 073039
[34] Tacchino F, Auffèves A, Santos M F, and Gerace D 2018 *Phys. Rev. Lett.* **120** 063604
[35] Zhang J W, Wang B, Yuan W F, Li J C, Bu J T, Ding G Y, Ding W Q, Chen L, Zhou F, and Feng M 2024 *Phys. Rev. Lett.* **132** 180401
[36] Hu M J, Hu X M, and Zhang Y S 2024 *Chin. Phys. Lett.* **41** 050302
[37] Wiseman H M and Milburn G J 2009 *Quantum Measurement and Control* (Cambridge University Press)
[38] Elouard C and Jordan A N 2018 *Phys. Rev. Lett.* **120** 260601
[39] Anka M F, de Oliveira T R, and Jonathan D 2021 *Phys. Rev. E* **104** 054128
[40] Ding X, Yi J, Kim Y W, and Peter T 2018 *Phys. Rev. E* **98** 042122
[41] Elouard C, Herrera-Martí D, Huard B, and Auffèves A 2017 *Phys. Rev. Lett.* **118** 260603
[42] Behzadi N 2021 *J. Phys. A* **54** 015304
[43] Ma Y H, Xu D, Dong H, and Sun C P 2018 *Phys. Rev. E* **98** 042112
[44] De B and Muralidharan B 2016 *Phys. Rev. B* **94** 165416
[45] Insinga A, Andresen B, and Salamon P 2016 *Phys. Rev. E* **94** 012119
[46] Roßnagel J, Abah O, Schmidt-Kaler F, Singer K, and Lutz E 2014 *Phys. Rev. Lett.* **112** 030602
[47] Su S H, Chen J F, Ma Y H, Chen J C, and Sun C P 2018 *Chin. Phys. B* **27** 060502
[48] Klatzow J, Becker J N, Ledingham P M, Weinzetl C, Kaczmarek K T, Saunders D J, Nunn J, Walmsley T A, Uzdin R, and Poem E 2019 *Phys. Rev. Lett.* **122** 110601
[49] Korzekwa K, Lostaglio M, Oppenheim J, and Jennings D 2016 *New J. Phys.* **18** 023045
[50] Francica G, Binder F C, Guarnieri G, Mitchison M T, Goold J, and Plastina F 2020 *Phys. Rev. Lett.* **125** 180603
[51] Liu D H, Hong Y Y, Luo S L, He X, Wu Z Q, and Wang J H 2025 *Phys. Rev. A* **111** 012203
[52] de Assis R J, de Mendonça T M, Villas-Boas C J, de Souza A M, Sarthour R S, Oliveira I S, and de Almeida N G 2019 *Phys. Rev. Lett.* **122** 240602
[53] Lloyd S 2000 *Phys. Rev. A* **62** 022108
[54] Vanderbruggen T, Kohlhaas R, Bertoldi A, Bernon S, Aspect A, andragin A, and Bouyer P 2013 *Phys. Rev. Lett.* **110** 210503
[55] Lin Z Y, Su S H, Chen J Y, Chen J C, and Santos J F G 2021 *Phys. Rev. A* **104** 062210
[56] Chen L, Yan D, Song L J, and Zhang S 2019 *Chin. Phys. Lett.* **36** 030302
[57] Yamamoto N 2014 *Phys. Rev. X* **4** 041029
[58] Jacobs K, Wang X, and Wiseman H M 2014 *New J. Phys.* **16** 073036
[59] Wang W B, Chang X Y, Wang F, Hou P Y, Huang Y Y, Zhang W G, Ouyang X L, Huang X Z, Zhang Z Y, and Wang H Y 2018 *Chin. Phys. Lett.* **35** 040301
[60] Landauer R 1961 *IBM J. Res. Dev.* **5** 183
[61] Sagawa T 2012 *Thermodynamics of Information Processing in Small Systems* (Springer Tokyo)
[62] Goold J, Paternostro M, and Modi K 2015 *Phys. Rev. Lett.* **114** 060602
[63] Vu T V and Saito K 2022 *Phys. Rev. Lett.* **128** 010602
[64] Allahverdyan A E and Nieuwenhuizen T M 2001 *Phys. Rev. E* **64** 056117
[65] Proesmans K, Ehrich J, and Bechhoefer J 2020 *Phys. Rev. Lett.* **125** 100602
[66] Lorenzo S, McCloskey R, Ciccarello F, Paternostro M, and Palma G M 2015 *Phys. Rev. Lett.* **115** 120403
[67] Xi M M, Wang J R, Lu J C, and Jiang J H 2021 *Chin. Phys. Lett.* **38** 088801
[68] Dann R and Kosloff R 2020 *New J. Phys.* **22** 013055
[69] Feyisa C G and Jen H H 2024 *New J. Phys.* **26** 093039
[70] Uzdin R, Levy A, and Kosloff R 2015 *Phys. Rev. X* **5** 031044
[71] Peterson1 J P S, Batalhão T B, Herrera M, Souza A M, Sarthour R S, Oliveira I S, and Serra R M 2019 *Phys. Rev. Lett.* **123** 240601
[72] Lloyd S 1997 *Phys. Rev. A* **56** 3374
[73] Abdi M, Degenfeld-Schonburg P, Sameti M, Navarrete-Benlloch C, and Hartmann M J 2016 *Phys. Rev. Lett.* **116** 233604
[74] Scully M O and Zubairy M S 1997 *Quantum Optics* (Cambridge University Press, Cambridge)
[75] Weiss U 2012 *Quantum Dissipative Systems* (World Scientific, Singapore)
[76] Breuer H P and Petruccione F 2002 *The Theory of Open Quantum SystemsThe Theory of Open Quantum Systems (Oxford University Press on Demand, New York)* (Oxford University Press on Demand, New York)
[77] See Supplemental Material for detailed derivations and discussions on Measurement-Conditioned Coherent Control: Driving-Speed and Measurement-Basis Optimization in Quantum Heat Engines
[78] Kosloff R and Rezek Y 2017 *Entropy* **19** 136

[79] Although the energy change induced by the projective measurement may formally be classified as either work or heat [51], we identify it as heat because it originates from stochastic measurement backaction at a fixed Hamiltonian and is accompanied by entropy production. Treating this energy increase as work implies $\sum_m W_{\mathrm{p}}^m + W_{\mathrm{mea}} < 0$. Consequently, this implies that net work is performed on the system by the measurement device, in which case the cycle would no longer operate as a heat engine.

[80] During the isochoric cooling stroke, heat exchange Q_{c} with the cold reservoir is determined by the energy difference for each measurement outcome as follows: $Q_{\mathrm{c}} = \sum_{m=\pm} q_m \left(E_{t_0} - E_{t_3^m}\right)$, where $E_t = \mathrm{Tr}(\rho_t H(t)]$ is the system energy under the constant Hamiltonian $H(t) = \omega\sigma_x/2$. This satisfies $Q_{\mathrm{c}} + Q_{\mathrm{me}} + W = 0$ because of the cyclic return to the initial state, thus confirming energy conservation for the qubit. Furthermore, $Q_{\mathrm{c}} < 0$ holds consistently, thereby indicating net heat flow into the cold reservoir.